WILEY

RESEARCH ARTICLE

Expression dynamics and physiologically relevant functional study of STEVOR in asexual stages of *Plasmodium falciparum* infection

Himanshu Singh[1,2,6] (iD) | Kripa Madnani[3]* | Ying Bena Lim[1,2]* | Jianshu Cao[2,4] |
Peter R. Preiser[2,3] | Chwee Teck Lim[1,2,5]

[1] Department of Biomedical Engineering, National University of Singapore, Singapore

[2] Infectious Diseases IRG, Singapore-MIT Alliance for Research and Technology, Singapore

[3] School of Biological Sciences, Nanyang Technological University, Singapore

[4] Department of Chemistry, Massachusetts Institute of Technology, Cambridge, Massachusetts, USA

[5] Mechanobiology Institute, National University of Singapore, Singapore

[6] Wellcome Trust Centre for Molecular Parasitoogy, University of Glasgow, Glasgow, UK

Correspondence
Chwee Teck Lim, Infectious Diseases IRG, Singapore-MIT Alliance for Research and Technology, 138602 Singapore.
Email: ctlim@nus.edu.sg

Peter R. Preiser, Department of Biomedical Engineering, National University of Singapore, 119615 Singapore.
Email: prpreiser@ntu.edu.sg

Abstract

The extensive modification of *Plasmodium falciparum*-infected erythrocytes by variant surface antigens plays a major role in immune evasion and malaria-induced pathology. Here, using high-resolution microscopy, we visualize the spatio-temporal expression dynamics of STEVOR, an important variant surface antigens family, in a stage-dependent manner. We demonstrate that it is exported to the cell surface where protein molecules cluster and preferentially localize in proximity to knobs. Quantitative evidence from our force measurements and microfluidic assays reveal that STEVOR can effectively mediate the formation of stable, robust rosettes under static and physiologically relevant flow conditions. Our results extend previously published studies in *P. falciparum* and emphasize the role of STEVOR in rosetting, an important contributor to disease pathology.

1 | INTRODUCTION

During its 48-hr asexual life cycle, the *Plasmodium falciparum* parasite invades red blood cells (RBC), multiplies within them, and finally egresses to reinvade fresh RBC in an iterative cycle (Wirth, 2002). During these stages, the parasite exports various proteins to the RBC cytoplasm and beyond. Export of variant surface antigens (VSA) constitutes a crucial mechanism employed by the parasite to successfully evade the host immune system and establish a long-lasting chronic infection (Gardner et al., 2002; Kaviratne, Khan, Jarra, & Preiser, 2002; Lowe, Mosobo, & Bull, 1998). Studies have also suggested that VSA play a critical role in parasite-mediated pathology (Buffet et al., 1999; Dzikowski, Templeton, & Deitsch, 2006; Fernandez, Hommel, Chen, Hagblom, & Wahlgren, 1999; Rowe, Moulds, Newbold, & Miller, 1997; Subudhi et al., 2015; Warimwe et al., 2012). Three large exported multigene families have been identified in *P. falciparum* (Gardner et al., 2002; Lavazec, Sanyal, & Templeton, 2006). They are

the *var*-encoded *P. falciparum* erythrocyte membrane protein 1 (PfEMP1), the repetitive interspersed family (*rif*)-encoded RIFIN proteins, and the subtelomeric variant open reading frame (*stevor*)-encoded STEVOR proteins. To date, most studies have focused on PfEMP1 and have shown that the ligand plays a critical role in important pathological attributes of the disease including microvasculature obstruction, by binding to different receptors on endothelial cells (Baruch, Gormely, Ma, Howard, & Pasloske, 1996; Baruch et al., 1997; Buffet et al., 1999) as well as on uninfected RBC (uRBC) (Chen et al., 1998; Rowe et al., 1997). RIFINs, the second largest group of VSA, are known to be expressed on the infected RBC (iRBC) surface at the asexual stages (Goel et al., 2015; Kyes, Rowe, Kriek, & Newbold, 1999). Their role in PfEMP1-independent rosetting by binding to the group A antigen on the surface of uRBC and thus contributing to microvascular obstruction has been recently demonstrated (Goel et al., 2015).

Stevor genes, located at the subtelomeric ends of the parasite's chromosomes along with the *rif* and *var* multigene family (Gardner et al., 2002; Kaviratne et al., 2002; Lavazec et al., 2006), constitute the third largest variant antigen family of *P. falciparum*. The ~40-member family codes for proteins with an approximate molecular weight of 40 kD. STEVOR has been shown to be expressed during the asexual, gametocyte, and sporozoite stages of the *P. falciparum* life cycle (Niang et al., 2014; Khattab et al., 2008; Khattab & Meri, 2011; McRobert et al., 2004), suggesting that these proteins have multiple roles. At the gametocyte stages, STEVOR has been shown to be associated with the iRBC membrane (McRobert et al., 2004) and to directly impact the mechanical properties of the cell by increasing the membrane rigidity (Tiburcio et al., 2012). At the asexual stages, STEVOR, like PfEMP1 and RIFIN, is localized to Maurer's Clefts (Kaviratne et al., 2002), the organelles that are involved in the assembly and transport of the cytoadherence complex (Wickert, Göttler, Krohne, & Lanzer, 2004). In addition, a fraction of STEVOR is exported to the iRBC surface (Lavazec et al., 2006; Niang et al., 2014), resulting in an increase in membrane rigidity (Sanyal et al., 2012). While it is currently not clear whether all members of STEVOR have the same function during parasite maturation, Niang *et al.* showed that a number of different STEVOR can directly mediate binding to glycophorin C and that surface expression of STEVOR on the iRBC was able to directly mediate rosetting by engaging glycophorin C on the surface of uRBC (Niang et al., 2014). At this stage, the export dynamics of STEVOR as well as its arrangement on the iRBC surface are not understood. Critically, the relevance of STEVOR-mediated rosetting under physiological conditions is also not clear.

In this study, using a combination of high-resolution molecular force spectroscopy and immunogold electron microscopy, we demonstrate the surface expression dynamics of STEVOR at different stages during maturation of the asexual parasite. By combining dual-micropipette force and microfluidics-based rosetting assays, we are able to quantitatively assess the contribution of STEVOR in the formation of rosettes. These results highlight the functional importance of STEVOR proteins in physiologically relevant conditions and improve the understanding of the STEVOR surface expression and its role at asexual stages of parasite infection.

2 | RESULTS

2.1 | Characterization of strains

To systematically study the expression and functional aspects of STEVOR, parasite clones with known expression levels of STEVOR were utilized. The A4 clone has been shown to be STEVOR deficient (Niang et al., 2014), and the 3D7-derived 5A clone is known to express high levels of STEVOR (Niang, Yam, & Preiser, 2009). In addition, A4 was transfected with two STEVOR genes (PFF_0850c and PF10_0395) to generate A4(tr-I) and A4(tr-II) clones, respectively, with A4(tr-II) expressing a GFP-tagged STEVOR (Niang et al., 2014). All these clones were characterized for STEVOR expression by immunofluorescence assay (IFA) and showed the expected location pattern. Critically, STEVOR surface expression was clearly established for all the different STEVOR-expressing clones used (Figure S1).

2.2 | STEVOR accumulates on the surface of late-stage iRBC in a stage-dependent manner

To study the pattern and distribution of exposed STEVOR proteins on the infected erythrocyte surface, atomic force microscopy (AFM)-based force mapping was used. AFM can detect molecular events at high resolution (Dammer et al., 1996; Florin, Moy, & Gaub, 1994; Lee, Kidwell, & Colton, 1994). Our set-up comprised an anti-STEVOR antibody (anti-S1 serum) functionalized AFM tip (spring constant 0.01 N/m) that was used to probe the asexual iRBC surfaces (Figure 1(a)). The adhesive interactions between protein-antibody molecular pairs, if any, were quantified as force histograms and spatial adhesion force maps. The protocol was validated and standardized with a combination of control experiments (Data S1; Table S1).

Based on the data from control experiments (Data S1), a detachment force of 20 pN was set as an appropriate threshold to eliminate signal noise and nonspecific interactions. Adhesive interactions with detachment force >20 pN were classified as relevant adhesion events (for details, see Data S2; Figures S2 and S3). These events were integrated, and the final adhesion maps were generated.

Specific adhesion frequency was defined as the percentage of relevant adhesion events amongst all probing interactions and has been compared amongst different clones in Figure 1(b). 5A clone iRBC showed 60 ± 3.7% specific adhesion frequency. The transfection of the A4 clone with STEVOR genes significantly increased the occurrence of specific adhesion events to 52.1 ± 3.4% and 67.4 ± 4.0% in A4(tr-I) and A4(tr-II) clones, respectively, as opposed to 4.6% in A4. An anti-ATS antibody, against the intracellular domain of PfEMP1, was used as another negative control to ensure only surface probing of iRBC. Late-stage iRBC from the 5A clone, probed with anti-ATS antibody functionalized AFM tips, showed specific adhesion frequency of 4.2 ± 0.5%, which was quite similar to that of the STEVOR-deficient clone A4.

To analyze the surface expression levels of STEVOR proteins in a stage-dependent manner, the entire set of force scans from 5A, A4(tr-I), and A4(tr-II) populations was grouped into trophozoite and schizont stages. Twenty force map scans of ring-stage iRBC (10 from 5A and five each from A4(tr-I) and A4(tr-II)) were also included.
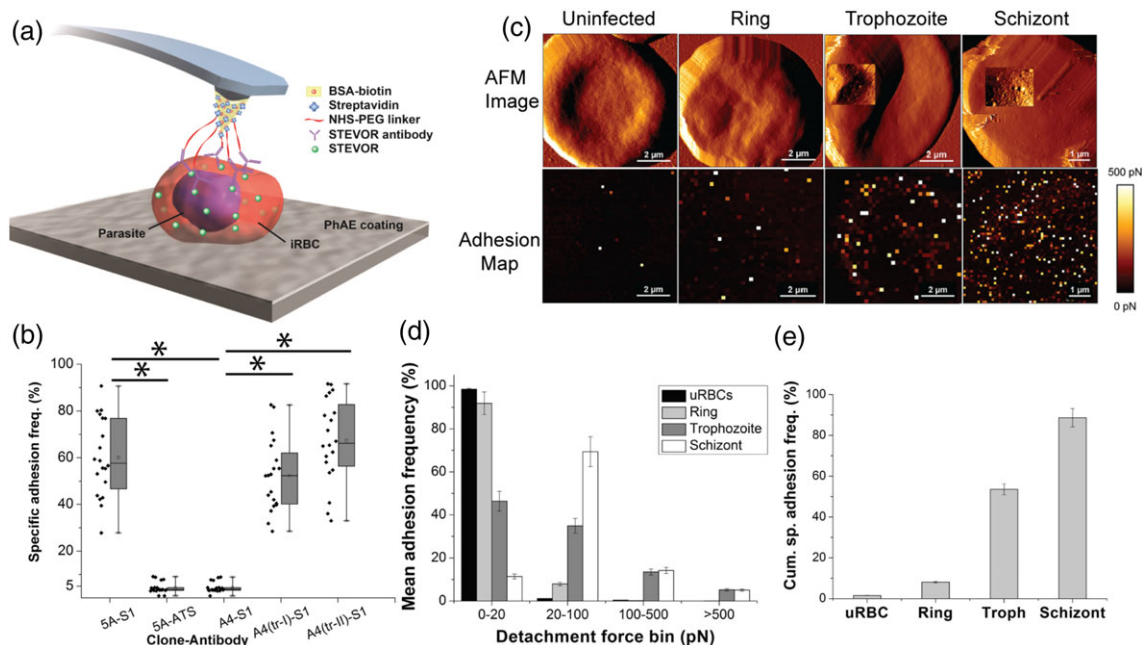
FIGURE 1 STEVOR on infected red blood cells (iRBC) surface. (a) Basic schematic of the force mapping technique. (b) Specific adhesion frequency distribution for all clones (*p << 0.01). (c) Representative atomic force microscopy (AFM) reconstructed images and corresponding adhesion force maps of cells. The first row shows the AFM-scanned surface images of iRBC in the scanned area, and the second row shows the corresponding spatial distribution of adhesive interactions between the functionalized tip and the scanned area (cell surface and beyond). The color of adhesion spots reflects the strength of adhesive force at that location. A small number of nonspecific adhesive interactions were observed outside the cell surface area that were manually isolated in offline data processing and were not considered in the quantification of specific interactions between cell surface and antibody functionalized AFM tip. Inset areas in third and fourth column of the first row show the zoom in view on the surface of the scanned late-stage iRBC. Knobby protrusions can be clearly observed on the cell surface. Cells presented are representative of the majority of the cell population set. (d) Bin-wise distribution of mean adhesion frequency for iRBC at different stages of infection. Error bar: standard error of mean. (e) Cumulative specific adhesion frequency in population sets of uninfected, ring, trophozoite, and schizont red blood cells. Data: mean ± standard error of mean

Figure 1(c) shows the compilation of the spatial adhesion maps of distinct iRBC at progressive asexual stages. Data for the uRBC set was collected from one of the controls (Data S1). The adhesion force maps reflected the stage-dependent change in the distribution density of adhesion events and their associated detachment strengths. Figure 1(d) shows the bin-wise distribution of these forces at different stages (Table S2). In summary, the total specific adhesion frequency was observed to increase from 8.1 ± 0.4% (ring) to 53.6 ± 2.7% (trophozoites) and 88.63 ± 4.4% (schizont) (Figure 1 (e)). This clearly reflects a consistent increase in the surface expression levels of STEVOR on the iRBC as the parasite develops within it from late ring to mature schizont.

2.3 | STEVOR clusters on the iRBC surface in close proximity to knobs

Force mapping experiments also revealed an interesting insight about the clustering behavior of STEVOR molecules on the iRBC surface. Scans of iRBC at 64 × 64 pixels revealed multiple large force adhesion events in a substantial fraction of retraction force curves as well as continuous patches of large adhesion in various regions on iRBC surface (Figure 2(a)). To further investigate these events and to get detailed insights about whether these proteins clustered on the cell surface, a total of 15 schizont iRBC were first examined (five each from 5A, A4(tr-I), and A4(tr-II)) at 64 × 64 pixels. From each scan, a unit area

region (1 × 1 μm) of suspected high adhesion was selected and was further probed at 128 × 128 pixels (Figure 2(b)), collecting a total of around 2×10^5 curves at a spatial resolution of around 8 nm. Approximately 57% of these force curves showed multiple bond rupture events during the retraction phase (Figure S4). This indicated the presence of multiple STEVOR molecules in these 8 × 8 nm nanoscale regions. Around 92.5% of 1.14×10^5 selected force curves (57% of 2×10^5 total force curves mentioned above) were indicative of two or more STEVOR molecules being present in probing region.

The spatial distribution of STEVOR was also analyzed by immunogold electron microscopy of iRBC. Figure 2(c) shows the normal and backscatter scanning electron microscope (SEM) images of a late-stage iRBC from the 5A clone. Here, STEVOR molecules on the cell surface were immunostained with an anti-S1 serum followed by secondary antibodies conjugated with 10-nm gold (Au) nanoparticles (Figures 2(c), S5, and S6(a)). These images revealed that STEVOR were distributed on the surface in various cluster sizes. Images from pre-embedding immuno-TEM of iRBC showed clusters of gold nanoparticles on the extracellular surface of cells and post-embedding immuno-TEM of fixed iRBC revealed localizations of Au nanoparticles in different parts of the cell—Maurer's Clefts, RBC membrane, and cell surface (Figures 2(d,e), S6(b,c), and S7), which are consistent with previous findings (Blythe et al., 2008; Lavazec et al., 2006) and our IFA results. Statistical quantification of TEM images from a total of 100 late-stage iRBC (5A, A4(tr-I and II)) suggested that around 73.48% of
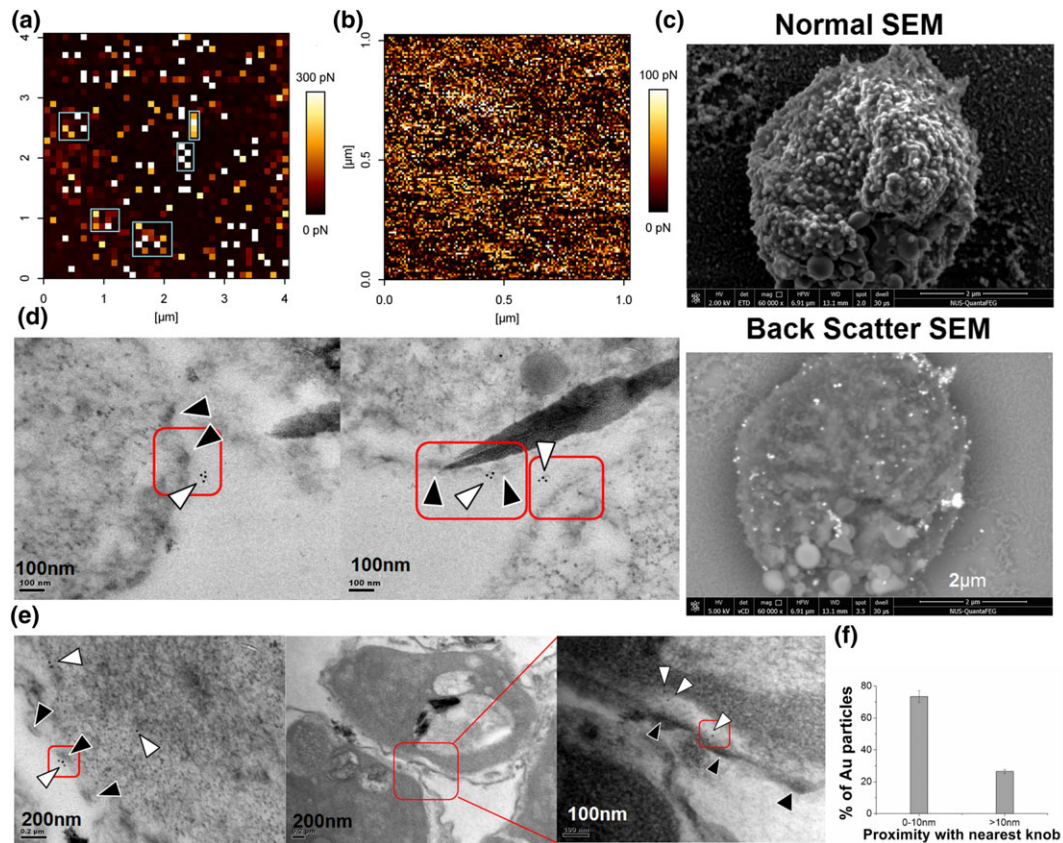
FIGURE 2 Clustering of surface-exposed STEVOR in proximity to knobs. (a) Adhesion map of a 4 × 4-μm region on an infected red blood cells (iRBC) surface at 64 × 64 pixels (White boxes—areas of strong adhesion). (b) Adhesion force map of a typical 1 × 1-μm region on an iRBC surface at 128 × 128 pixels. Multiple bright spots with detachment forces as high as 400 pN were observed. (c) Normal and backscatter scanning electron microscope images of a typical late-stage iRBC from a 5A clone. The normal image shows the surface topology, whereas the backscatter image shows the bright 10-nm gold nanoparticles. Scale bar: 2 μm. (d) Representative images from pre-embedded transmission electron microscopy imaging of ultra-thin slices (~90 nm) of late-stage 5A iRBC. Gold particle clusters can be observed in proximity to surface knobs of cells. White arrows: 10-nm Au particles; black arrows: knobs. (e) Representative images from post-embedded transmission electron microscopy imaging of ultra-thin slices (~90 nm) of late-stage 5A iRBC. The third image in the row shows the zoom in view of the red highlighted region in the second image. Gold tagged STEVOR can be observed in different parts of the cell and in close proximity to surface knobs in the near-surface region. Scale bars have been indicated in images. (f) Statistical quantification reveals preferential localization of Au nanoparticles in proximity to knobs. Error bar: standard error of mean

the Au nanoparticles conjugated to the iRBC membrane were localized within 0–10 nm from the nearest knob (Figure 2(f)).

2.4 | STEVOR mediates stable rosetting in static conditions

To investigate the functional role of STEVOR in rosetting interactions, static rosetting assays were established with enriched rosetting-positive (R+) cultures of all four clones—5A, A4, A4(tr-I), and A4(tr-II). The rosetting ability of these parasites was quantified in terms of rosetting frequency (RF), that is, the fraction of iRBC involved in the formation of stable rosettes. Antibody-mediated inhibition assays were also performed with all clones by pre-incubating the R+ iRBC populations with the anti-S1 serum (1 hr, 37°C) before setting up the rosetting assays. Table 1(a) shows the summary of RF scores and % of rosette with size ≥3 for all clones in rosetting and inhibition assays. Rosetting assays were performed in duplicates for each clone and were repeated five times.

To quantitatively probe the contribution of STEVOR in rosetting, dual-micropipette aspiration-based force assays (Nash, Cooke, Carlson, & Wahlgren, 1992b) were performed with all four clones in rosetting and inhibition assays. The basic schematic of the force assay is shown in Figure 3(a). Each rosette was held with one pipette, and attached uRBC were sequentially aspirated with a second pipette (Figure 3(b)). Aspiration pressure was monitored as voltage output from the pressure transducer. This voltage was later converted to suction pressure using the calibration chart (Figure S5). The mean binding force for a rosette was computed as the average of aspiration forces required to detach all uRBC in that cluster. Table 1(b) shows the summary of mean rosette binding forces for all clones in the two assays, and Figure 3(c) shows the statistical comparison of these forces. As observed from the table, STEVOR +ve clones exhibited much stronger (~4 times) rosette binding forces as compared to that of A4. This shows that STEVOR can effectively and stably modulate the rosetting strength of parasites. Isotype serum pre-incubation had no observable effect on the strength of the formed rosettes (data not shown). In order to investigate whether disrupted rosettes could reform, iRBC

TABLE 1 Comparison of rosetting frequency, size, and rosette strengths for all clones

| | A | | | B | |
| | RF score (%) (n = 5) | | % of rosettes with size ≥ 3 | Mean rosette binding force (pN) | |
Clone	Rosetting assay	Inhibition assay		Rosetting assay	Inhibition assay
5A	70.6 ± 4.5	25.8 ± 3.9	93.5	m = 30 530 ± 90	140 ± 50
A4(tr-I)	55.8 ± 4.1	17.8 ± 3.1	86.7	430 ± 80	180 ± 30
A4(tr-II)	60.8 ± 6.7	14.9 ± 4.1	96.4	510 ± 80	130 ± 40
A4	3.8 ± 1.5	3.6 ± 1.8	31.5	m = 10 90 ± 10	90 ± 20

Note. Rosetting assays were performed in duplicate for each clone and were repeated five times.

For force assays, 30 rosettes from each of the 5A, A4(tr-I), and A4(tr-II) clones were tested in a total of four different experiments. Only 10 rosettes could be tested with an A4 clone in a total of four different experiments.

Data is presented as mean ± SD.

*n*: no. of independent experiments; *m*: no. of rosettes analyzed; RF: rosetting frequency.

from disrupted rosettes were brought back into contact with fresh uRBC in the same sample. The cells, held in micropipettes, were brought in contact for a certain time, and the uRBC were aspirated.

This was repeated with each cell pair for different contact durations between the iRBC and the uRBC. Even with small contact duration of 2–3 min, the cells under test were observed to adhere to each other. However, such contacts were not stable and adhesion forces were found to fluctuate. With regular increment in contact duration, these binding forces increased rapidly with values stabilizing close to the original binding strength after 30–40 min of contact (Figure 3(d)).

2.5 | STEVOR mediates robust rosetting in physiological flow

To test whether STEVOR proteins were capable of forming rosettes under flow conditions, microfluidics-based rosetting assays were established with R+ sets of 5A, A4, and A4(tr-I and II) clones. As the late-stage iRBC in *P. falciparum* sequester in blood vessels and disappear from circulation (Hasler et al., 1990; Rowe, Obiero, Marsh, & Raza, 2002), it is reasonable to assume that rosette formation in flow conditions is initiated around these adhered iRBC. Hence, a similar *in vitro* environment was replicated in our flow-rosetting assays. The overall schematic of the assay is shown in Figure 4(a). Under 0.1–0.2 Pa laminar shear flow, rosettes of different sizes could be observed with R +5A and R+A4(tr-I and tr-II) parasites, whereas R+A4 parasites failed to form stable rosettes in this flow environment (Figure 4(b)). Figure 4(c) shows the time-dependent response of different clones as
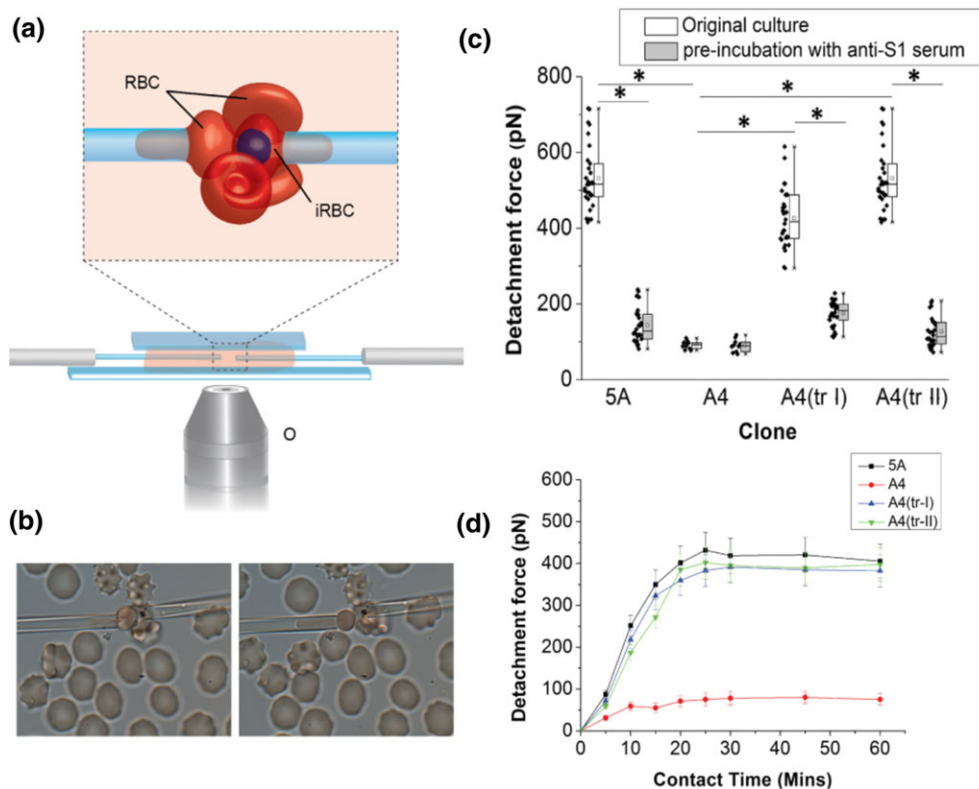
FIGURE 3 STEVOR can quantitatively modulate the strength of rosettes. (a) A schematic demonstrating the dual-micropipette force assay technique. (b) Microscopic images of a typical rosette during probing of cell–cell adhesion force. (c) Comparison of mean binding strength of rosettes formed by clones—5A, A4, A4(tr-I), and A4(tr-II) clones in normal and pre-blocked rosetting assays. Each data point shows the binding strength of one rosette. Thirty rosettes from each of the 5A, A4(tr-I), and A4(tr-II) clones were tested in a total of four different experiments, whereas with the A4 clone, only 10 rosettes could be tested in a total of four different experiments. Upper and lower limits of boxes show the 25th and 75th percentile, respectively, and whiskers show the extreme values of each side of the box. An asterisk shows the significance level of $p << 0.01$. (d) Time-dependent rosette binding forces in reformation assays. Data: mean ± standard error of mean; 10 cell pairs for each time point in a total of three different experiments. iRBC, infected red blood cells
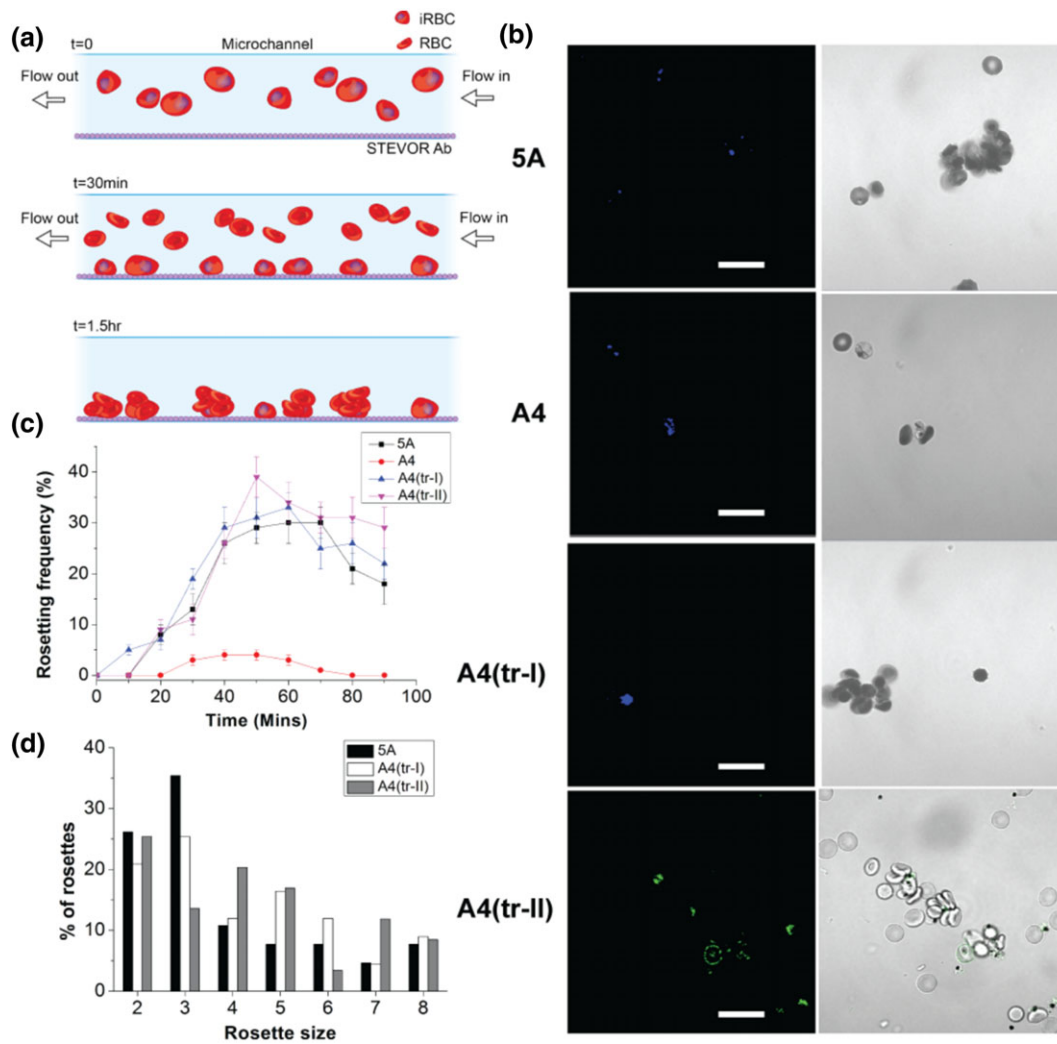
FIGURE 4 STEVOR can mediate rosetting under flow conditions. (a) A schematic of microfluidics rosetting assay. Enriched R+ infected red blood cells (iRBC) were injected in the channel and allowed to adhere on the anti-S1 serum-coated surface. Subsequently, fresh-flowing uninfected RBC were allowed to interact with adhered iRBC. (b) Representative images of rosettes during flow assays for all four clones. The first column shows the DAPI stain for the first three clones and shows the GFP STEVOR for the last row (A4(tr-II) clone); the second column shows the bright field images of cells. Scale bar: 20 μm. (c) Plot showing the real-time rosetting behavior of the four clones in flow assay. Data from at least two independent experiments. Error bar: standard error of mean. (d) Steady state size distribution of rosettes formed by different clones in the flow channel

the uRBC flowed by and interacted with adhered iRBC. As is clear from the graph, iRBC from 5A, A4(tr-I), and A4(tr-II) clones showed a similar time-dependent trend of RF, which increased with time and reached to a plateau after 50–60 min from the start of uRBC flow. For the 5A clone, 30 ± 3.4% plateau RF was observed after around 50–60 min. Similar responses were obtained with A4(tr-I) and A4(tr-II) clones that exhibited around 33 ± 4.7% and 39 ± 4.2% plateau (RF), respectively, after around 50–60 min. With the A4 clone, 4% peak RF was observed after around 30–40 min. However, these clusters were transient in nature and mostly disrupted within the next 5–10 min. Figure 4(d) shows the size distributions of stable rosettes formed by clones 5A, A4(tr-I), and A4(tr-II) after 60 min. The relatively lower yield of rosettes observed in these flow assays, as compared to static assays, could be attributed to a number of factors. Firstly, in order to image the channel sections clearly, the concentration of fresh uRBC in flow was kept lower. This significantly reduced the uRBC/iRBC ratio in the flow assay. The unidirectional flow in the assay also reduced the iRBC–

uRBC interaction time, leading to a lower binding probability between cells. Also, the pre-adherence of cells to the channel bed decreased the exposed surface area and hence the available STEVOR content on the surface. Taken together, these assays suggest the direct involvement of surface expressed STEVOR in mediating the stable and robust rosetting interactions under static and dynamic conditions in the A4 genetic background in vitro.

3 | DISCUSSION

The export of different variant antigen families by the *P. falciparum* parasite is a crucial survival strategy by which it can potentially evade the host immune system (Gardner, Pinches, Roberts, & Newbold, 1996; Rowe et al., 2002). The *var*, *rif*, and *stevor* constitute the three major parasite-derived variant surface antigen families in *P. falciparum* (Lavazec et al., 2006). Apart from the well-studied *var* gene-encoded

PfEMP1 proteins, only a limited number of studies have approached the detailed functional roles of the other antigen families (Goel et al., 2015; Niang et al., 2014; Sanyal et al., 2012; Tiburcio et al., 2012). Here, using a combination of high-resolution imaging techniques and quantitative biophysical assays on a set of STEVOR transfected and selected strains, we presented a detailed expression and functional characterization of two members of the STEVOR multigene family during the asexual stages of the parasite life cycle. Molecular force spectroscopy and immunogold labeling-based electron microscopy were first employed to map the distribution of STEVOR on the surface of late-stage iRBC. Subsequently, dual-pipette aspiration-based force assays and microfluidics-based rosetting assays were carried out. This was done in order to study the contribution of STEVOR to parasite rosetting as well as the relevance of STEVOR-mediated rosettes under physiological conditions. Our results suggest that, with parasite maturation, STEVOR accumulates on the surface of iRBC and forms clusters. Interestingly, a significant fraction of these clusters were observed to preferentially localize in proximity to the knobs. We also showed that STEVOR can mediate strong and stable rosetting under static as well as physiologically relevant flow conditions. Rosetting, an important adhesion phenotype of the disease, has been associated with complicated malaria in many clinical studies (Rowe, Obeiro, Newbold, & Marsh, 1995; Rowe et al., 2002). This phenomenon is believed to confer multiple advantages to the parasite. One hypothesis suggests that a rosette not only creates a shield for the maturing parasite to hide itself from immune cells, but also provides the emerging merozoites an easy access to fresh target uRBC (Rowe et al., 2002). However, this idea has been challenged by other studies wherein no direct correlation between the rosetting phenotype and parasitemia was observed (Clough, Atilola, & Pasvol, 1998). At the molecular level, thus far, PfEMP1 has been implicated as the major ligand involved in mediating the cytoadherence and rosetting of iRBC (Baruch et al., 1997; Chen et al., 1998; Rowe et al., 1997). However, the expression of PfEMP1-like proteins and endothelial sequestration has been largely restricted to P. falciparum malaria (Leech et al., 1984) while rosetting has been observed in all human malaria species as well as in simian and rodent malaria parasites (Doumbo et al., 2009; Lowe et al., 1998; Mackinnon, Walker, & Rowe, 2002; Udomsangpetch, Brown, Smith, & Webster, 1991). Importantly, while homologues of PfEMP1 have only been found in species such as Plasmodium knowlesi and Plasmodium reichenowi, homologues of small variant antigens such as STEVOR and RIFIN are present in almost all parasite species. In fact, other species of Plasmodium have been shown to have an even larger repertoire of small variant antigens, the best studied examples of which are the Plasmodium Interspersed Repeats (PIRs) found in rodent parasites as well as Plasmodium vivax and P. knowlesi (Jemmely, Niang, & Preiser, 2010). In addition, it has been shown in earlier studies that during the disease, each iRBC expresses only a single member of the PfEMP1 family that mediates a specific adhesion phenotype (Baruch et al., 1997; Howell et al., 2008). Assuming PfEMP1 to be the sole mediator of adhesive interactions of the iRBC, this exclusive nature of the PfEMP1 expression would imply that, at a given time, a single iRBC can either form a rosette or cytoadhere onto the endothelial cell wall. A recent study attempts to show the dual capability of a PfEMP1 variant in mediating rosetting and cytoadherence simultaneously (Adams,

Kuhnrae, Higgins, Ghumra, & Rowe, 2014). They show that iRBC from the IT/R29 strain, expressing a rosette-mediating PfEMP1 variant (IT4var09), cytoadhere in vitro to a human brain microvascular endothelial cell line (HBEC-5i) in static conditions. However, both the extent and the strength of cytoadherence between the iRBC and endothelial cells were observed to be extremely low in physiological flow conditions. However, coexpression of rosetting and cytoadherence receptors on the same P. falciparum iRBC, as observed in some clinical studies (Hasler et al., 1990), suggests that an individual iRBC can express multiple surface ligands simultaneously. Other recent studies have also implicated certain members of STEVOR and RIFIN variant antigen families in mediating the rosetting of the P. falciparum parasite (Goel et al., 2015; Niang et al., 2014) in a PfEMP1-independent manner. Therefore, the adhesive properties of rosetting and cytoadherence of the P. falciparum parasite may not be regulated by a single variant antigen group, but are probably the combined effect of different variant antigen families transported to the surface of the iRBC.

An important quantitative aspect of our work is the demonstration of the fact that STEVOR can independently generate a binding force of 400 ± 80 pN in a rosette (for details, see Data S3). This value is comparable to the rosette binding strength of 440 ± 130 pN, as observed in one of the earlier studies (Nash et al., 1992b). In another study, average detachment forces of ~100 pN were observed between iRBC and cultured endothelial cells lines expressing CD36 and ICAM-1 (Nash et al., 1992a). A more recent study quantifies the average adhesive forces between FCR3CSA late-stage iRBC and CSA-expressing CHO cells to be in the range of 100–200 pN (unpublished data). These comparisons suggest that STEVOR-mediated rosettes are more stable and robust, with much higher binding forces as compared to forces in endothelial sequestration.

The systematic export of different antigen groups in a regulated, timely manner can be of significant importance in disease pathology. Results from our AFM experiments suggest that STEVOR begins to appear on the iRBC surface from the trophozoite stage (~22 hr post infection) onwards, which is consistent with earlier transcriptional profiling data (Kaviratne et al., 2002; Lavazec et al., 2006). This surface expression constantly increases up to the mature schizont stage. PfEMP1 has been shown to be exported to the surface from as early as 16 hr post infection (Gardner et al., 1996). The delayed export of STEVOR on the iRBC surface after PfEMP1 may provide an interesting insight into the time-dependent interplay between protein export machinery of the parasite and the adhesion phenotype exhibited by the parasite. It is likely that PfEMP1, with a variety of binding domains for endothelial receptors, appears first on the surface in order to enable the parasite to sequester within the microvasculature. STEVOR, exported later to the iRBC surface, can then mediate the formation of robust rosettes around these sequestered late-stage iRBC (Figure 5). This model is supported by findings from our force and microfluidics assays. Thus, the sequential export of these adhesins by the parasite can create a synergistic framework by which the parasite is able to avoid the splenic circulation and sustain the infection by easily accessing fresh uRBC from rosettes.

Reinforcement of cytoadherence may also be a possible advantage that the parasite may derive from proximity of surface-exposed STEVOR clusters to surface knobs. Earlier, knobs have been shown
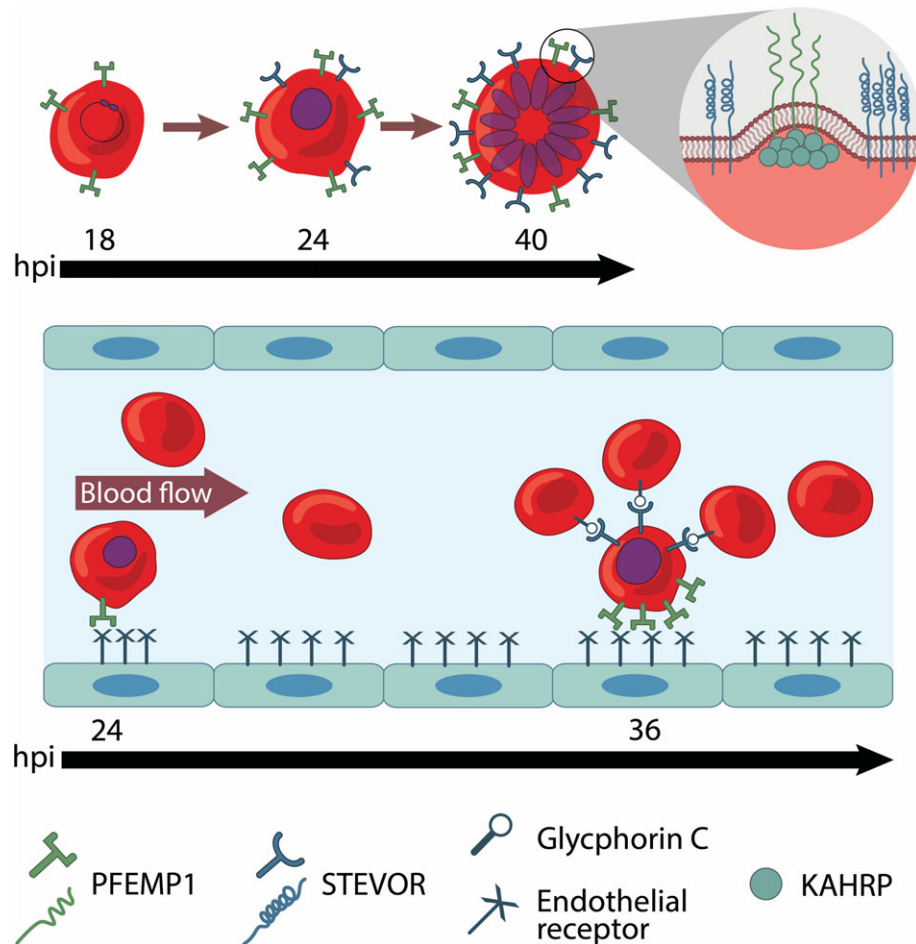
FIGURE 5 Proposed model to demonstrate time series of coordinated events in asexual life cycle. The first row in the cartoon graphics demonstrates the expression dynamics of STEVOR proteins on the surface of infected red blood cells (iRBC). STEVOR is progressively exported on the surface of the cell as the hour post infection (hpi) time line progresses. The zoom-in view shows the clustering of STEVOR in proximity to base of knobs. The second row depicts the time series of events occurring in blood flow. PfEMP1, first exported to the iRBC surface, mediate the sequestration of the cell to the endothelium. STEVOR, exposing on the surface of the sequestered iRBC, may potentially bind to receptors on passing by uninfected red blood cells and mediate the formation of rosettes around these adhered iRBC

as the contact points between sequestered iRBC and endothelial cells (Horrocks et al., 2005). At the very late asexual stage, the iRBC cytoskeleton degrades and dismantles in terms of network integrity and spectrin mesh sizes (Shi et al., 2013). This may affect the cytoadhesion strength, making it difficult for the parasite to remain adhered in shear flow. At this time, STEVOR, in proximity to knobs, may be utilized by the parasite to bind to certain receptors and provide extra anchoring support.

Within sites of sequestration, iRBC remain exposed to the host immune system for a period of 24+ hours. During this period, the host immune system can mount an effective adaptive immune response using antigens on the surface of these sequestered iRBC as targets. Enhancing the level of antigenic variation by exporting STEVOR to the iRBC surface may directly boost the immune evasion ability of the parasite, thus enabling it to safely reach maturity before bursting. However, the lack of sufficient evidence thus far in support of this hypothesis makes it an interesting avenue for future investigations.

Our work supports and extends previous studies and further substantiates the direct role of STEVOR parasite-mediated rosetting. However the data to date cannot rule out that STEVOR may also contribute to rosetting by other indirect mechanisms, like the rigidification of the iRBC membrane.

In conclusion, our work demonstrates the physiological importance of STEVOR at asexual stages of parasite development. Taken along with the known functions of other variant antigens, it outlines the context in which these various proteins interact and contribute to parasite-mediated pathology of *P. falciparum* malaria.

4 | EXPERIMENTAL PROCEDURES

4.1 | STEVOR antibodies

Anti-STEVOR polyclonal antibody (anti-S1 serum) was raised in rabbit against the N terminal conserved region of the gene PF10_0395. The details of antibody generation and specificity tests have been described elsewhere (Niang et al., 2009; Niang et al., 2014).

4.2 | Parasites, cultures, and transfections

A detailed description of deriving the 5A clone has been provided elsewhere (Niang et al., 2009). The A4 clone was a kind gift of Sue Kyes, Weatherall Institute of Molecular Medicine, Headington, Oxford, UK. The transfected A4 (tr-II) clone was previously described (Niang et

al., 2014) while clone A4(tr-I) was generated in our lab. The pARL plasmid-containing *stevor* (PFF0850C) gene under the control of the *hsp86* promoter of *P. falciparum* was transfected into the A4 parasite. Selection was carried out using 5 nM of WR99210 drug. Parasites were cultured in standard *in vitro* conditions (Niang et al., 2009). Late-stage iRBC were enriched using the Magnetic Sorting set up (MACS, Miltenyi). Experimental details for transfection of clones are available elsewhere (Niang et al., 2014).

4.3 | Immunofluorescence assay

For fixed IFAs, iRBC from clones 5A, A4, and A4-(tr-I) were enriched by magnetic purification (MACS), fixed with 4% paraformaldehyde for 15 min, permeabilized with Triton X100 (Sigma-Aldrich), and resuspended in 1% bovine serum albumin (BSA) in PBS. After incubating with BSA, the washed pellet was incubated with anti-S1 serum (1:200) at 37°C for 60 min under rotating conditions. The unbound serum was removed by washing the suspension three times with 1X PBS. The primary antibody was detected by incubation for 1 hr with Alexa 488-conjugated donkey anti-rabbit serum (1:500 dilution, Sigma-Aldrich) for A4 and A4(tr-I) clones and with phycoerythrin-conjugated goat ant- rabbit secondary antibody (vCell Science) for the 5A clone.

For live IFA of A4 and A4(tr-I), MACS purified cells were directly suspended in 1% BSA at 37°C for 30 min and washed. Next, the cells were incubated with an anti-S1 serum (1:200) at 37°C for 60 min under rotating conditions followed by incubation for 1 hr with Alexa 488-conjugated goat anti-rabbit serum (1:500 dilution, Sigma-Aldrich). For live IFA of A4(tr-II) strain, no STEVOR antibody incubations were performed.

Before imaging, cells from each clone were stained with 6-diaminido-2-phenylindole (DAPI, 2 mg/mL in PBS) for 10 min, followed by a wash with 1XPBS. Slides were mounted in VECTASHIELD (Vector Laboratories) and visualized under an confocal microscope (ZEISS).

4.4 | AFM experiments

Details of AFM experiments can be found in the Supporting Information. Briefly, AFM tips were functionalized with the antibody, and probed on the adhered cells in force mapping mode. Experiments were carried out in fluid using the NanoWizard II JPK AFM set up (JPK Instruments). Collected force curve scans were processed using JPK SPM software (JPK Instruments) to obtain the visual-quantitative information. Histograms were generated using ORIGIN 8.1 software.

4.5 | Immunolabeling-based electron microscopy

For immunogold electron microscopy, similar experimental procedures as described in published literatures were used (Horrocks et al., 2005; Lavazec et al., 2006). Briefly, for immunogold SEM, cells were partially fixed with 4% paraformaldehyde, stained with the anti-S1 serum (1:25, 1 hr, 37°C) followed by staining with goat anti-rabbit secondary antibody pre-conjugated with 10-nm gold nanoparticles (Ted Pella Inc.) (1:10, 1 hr, 37°C) and were then fixed again. Samples were then dehydrated, critical point dried, and coated with carbon layer prior to imaging using the QUANTA FEG 650 (FEI) system. For post-

embedding labeling-based immuno-TEM, cells were fixed as described above, post fixed with osmium tetroxide, dehydrated and embedded in LR White resin (London Resin). After sectioning, the ultra-thin slices on copper grids were immunostained in the exact same manner as for immunogold SEM. The grids having cell slices were finally stained with lead citrate and observed with an Erlangshen ES500W camera (Gatan, Inc.) on a JEM-1010 electron microscope (JEOL Inc.) at 80 kV. For pre-embedding immuno-TEM, unfixed cells were first stained with rabbit anti-S1 serum (1:10, 2 hr, 37°C) and then labeled with goat anti-rabbit secondary antibody pre-conjugated with 10-nm gold nanoparticles (Ted Pella Inc.) (1:10, 1 hr, 37°C). Labeled cells were fixed and processed as described for post-embedding immuno-TEM.

4.6 | Rosetting selection

Parasite cultures were repeatedly selected for rosetting phenotypes using standard protocols as described in previous literatures (Niang et al., 2014).The RF, that is, the fraction of the iRBC population involved in formation of stable rosettes, was quantified. Dual micropipette and flow assays were performed with clones that had been selected at least three times for rosetting. A4 parasites, even after multiple selections, yielded a very low rosetting frequency.

4.7 | Rosetting assays and antibody-mediated inhibition

These assays were performed as described earlier (Niang et al., 2014). Briefly, 20 μl of enriched iRBC were incubated with fresh RBC in a binding medium (RPMI + 20%FBS) under rotating conditions for 1 hr at 37°C. Blocking assays were carried out by pre-incubating the purified iRBC with anti-S1 serum for 1 hr at 37°C. The excess serum was washed with RPMI, and the iRBC were then mixed with fresh RBC under rotation for 1 hr at 37°C. For each assay, 100 iRBC were counted to get a RF score.

4.8 | Dual pipette assay

To measure the rosette binding strength, the dual-micropipette assay was used. Briefly, uRBC were pulled out individually from rosettes on the stage of an inverted IX71 microscope (Olympus) equipped with a CCD Digital FireWire Camera (Olympus) and detachment forces were measured. In each experiment, rosettes were manipulated with two micropipettes, each mounted on a micromanipulator. The left micropipette was further connected to an integrated pneumatic system consisting of an automated syringe pump (Harvard), manual suction syringe, two burette columns and a pressure sensor (Validyne). The right micropipette was connected to a reservoir PHD 2000 syringe pump (Harvard) that could be manually operated to create −ve pressure to hold a rosette in the micropipette.

4.9 | Microchannel fabrication

Microfluidic channels were fabricated using standard procedures of photolithography and replica molding of Polydimethylsiloxane (PDMS) polymer as described elsewhere (Xu et al., 2013).

4.10 | Flow assay

Before each experiment, the bottom surface of the flow channel was coated with an anti-S1 serum by incubating overnight at 4°C. Nonspecific binding sites were blocked with 1% BSA in PBS. During the assay, enriched R+ iRBC, suspended in a rosette binding medium, were first allowed to flow in at ~0.05 Pa for 15 min, followed by 30 min of static incubation at 37°C so that the cells could adhere well on channel surface. After washing loosely bound iRBC, fresh uRBC were injected in channel and were allowed to flow at ~0.1 Pa shear stress. Sections of the channel were imaged on the IX71 microscope (Olympus) (details are in the Supporting Information).

AUTHOR CONTRIBUTION

C. T. L., P. R. P., and H. S. conceived and designed the experiments. H. S., K. G. M., and Y. B. L. performed the experiments. H. S. analyzed the data. J. C., H. S., K. G. M., and Y. B. L. contributed reagents, materials, and analysis tools. H. S., K. G. M., Y. B. L., C. T. L., P. R. P., and J. C. wrote the paper. H. S. is involved in all experiments.

REFERENCES

Adams, Y., Kuhnrae, P., Higgins, M. K., Ghumra, A., & Rowe, J. A. (2014). Rosetting Plasmodium falciparum-infected erythrocytes bind to human brain microvascular endothelial cells in vitro, demonstrating a dual adhesion phenotype mediated by distinct P. falciparum erythrocyte membrane protein 1 domains. Infection and Immunity, 82, 949–959.

Baruch, D. I., Gormely, J. A., Ma, C., Howard, R. J., & Pasloske, B. L. (1996). Plasmodium falciparum erythrocyte membrane protein 1 is a parasitized erythrocyte receptor for adherence to CD36, thrombospondin, and intercellular adhesion molecule 1. Proceedings of the National Academy of Sciences of the United States of America, 93, 3497–3502.

Baruch, D. I., Ma, X. C., Singh, H. B., Bi, X., Pasloske, B. L., & Howard, R. J. (1997). Identification of a region of PfEMP1 that mediates adherence of Plasmodium falciparum infected erythrocytes to CD36: Conserved function with variant sequence. Blood, 90, 3766–3775.

Blythe J. E., Yam X.Y., Kuss C., Bozdech Z., Holder A. A., Marsh K., ... Preiser, P. R. (2008). Plasmodium falciparum STEVOR proteins are highly expressed in patient isolates and located in the surface membranes of infected red blood cells and the apical tips of merozoites. Infection and Immunity 76: 3329–3336.

Buffet, P. A., Gamain, B., Shceidig, C., Baruch, D., Smith, J. D., Hernandez-Rivas, R., ... Scherf, A. (1999). Plasmodium falciparum domain mediating adhesion to chondroitin sulfate A: A receptor for human placental infection. Proceedings of the National Academy of Sciences of the United States of America, 96, 12743–12748.

Chen, Q., Barragan, A., Fernandez, V., Sundstrom, A., Schlichtherle, M., Sahlen, A., ... Wahlgren, M. (1998). Identification of Plasmodium falciparum erythrocyte membrane protein 1 (PfEMP1) as the rosetting ligand of the malaria parasite P. falciparum. The Journal of Experimental Medicine, 187, 15.

Clough, B., Atilola, F. A., & Pasvol, G. (1998). The role of rosetting in the multiplication of Plasmodium falciparum: Rosette formation neither enhances nor targets parasite invasion into uninfected red cells. British Journal of Haematology, 100, 99–104.

Dammer, U., Hegner, M., Anselmetti, D., Wagner, P., Dreier, M., Huber, W., & Guntherodt, H.-J. (1996). Specific antigen/antibody interactions measured by force microscopy. Biophysical Journal, 70, 2437–2441.

Doumbo, O. K., Thera, M., Kone, A. K., Raza, A., Tempest, L. J., Lyke, K. E., ... Rowe, J. A. (2009). High levels of Plasmodium falciparum rosetting in all clinical forms of severe malaria in African children. The American Journal of Tropical Medicine and Hygiene, 81, 987–993.

Dzikowski, R., Templeton, T. J., & Deitsch, K. (2006). Variant antigen gene expression in malaria. Cellular Microbiology, 8, 1371–1381.

Fernandez, V., Hommel, M., Chen, Q., Hagblom, P., & Wahlgren, M. (1999). Small, clonally variant antigens expressed on the surface of the Plasmodium falciparum-infected erythrocyte are encoded by the rif gene family and are the target of human immune responses. The Journal of Experimental Medicine, 190, 1393–1404.

Florin, E. L., Moy, V. T., & Gaub, H. E. (1994). Adhesion forces between individual ligand-receptor pairs. Science, 264, 415–417.

Gardner, M. G., Hail, N., Fung, E., White, O., Berriman, M., Hyman, R. W., ... Barrell, B. (2002). Genome sequence of the human malaria parasite Plasmodium falciparum. Nature, 419, 498–511.

Gardner, J. P., Pinches, R. A., Roberts, D. J., & Newbold, C. I. (1996). Variant antigens and endothelial receptor adhesion in Plasmodium falciparum. Proceedings of the National Academy of Sciences of the United States of America, 93, 3503–3508.

Goel, S., Mia, P., Kirsten, M., Nicolas, J., Patricia, L., Akhouri, R. R., ... Wahlgren, M. (2015). RIFINs are adhesins implicated in severe Plasmodium falciparum malaria. Nature Medicine, 21, 314–317.

Hasler, T., Handunnetti, S. M., Aguiar, J. C., Van Schravendijk, M. R., Greenwood, B. M., Lallinger, G., ... Howard, R. J. (1990). In vitro rosetting, cytoadherence, and microagglutination properties of Plasmodium falciparum-infected erythrocytes from Gambian and Tanzanian patients. Blood, 76, 1845–1852.

Horrocks, P., Pinches, R. A., Chakravorty, S. J., Papakrivos, J., Christodoulou, Z., Kyes, S. A., ... Newbold, C. I. (2005). PfEMP1 expression is reduced on the surface of knobless Plasmodium falciparum infected erythrocytes. Journal of Cell Science, 118, 2507–2518.

Howell, D. P., Levin, E. A., Springer, A. L., Kraemer, S. M., Phippard, D. J., Schief, W. R., & Smith, J. D. (2008). Mapping a common interaction site used by Plasmodium falciparum Duffy binding-like domains to bind diverse host receptors. Molecular Microbiology, 67, 78–87.

Jemmely, N. Y., Niang, M., & Preiser, P. R. (2010). Small variant antigens and Plasmodium evasion of immunity. Future Microbiology, 5, 663–682.

Kaviratne, M., Khan, S. M., Jarra, W., & Preiser, P. R. (2002). Small variant STEVOR antigen is uniquely located within Maurer's clefts in Plasmodium falciparum-infected red blood cells. Eukaryotic Cell, 1, 926–935.

Khattab, A., & Meri, S. (2011). Exposure of the Plasmodium falciparum clonally variant STEVOR proteins on the merozoite surface. Malaria Journal, 10, 58.

Khattab, A., Bonow, I., Schreiber, N., Petter, M., Schmetz, C., & Klinkert, M. Q. (2008). Plasmodium falciparum variant STEVOR antigens are

expressed in merozoites and possibly associated with erythrocyte invasion. *Malaria Journal, 7*, 137.

Kyes, S. A., Rowe, J. A., Kriek, N., & Newbold, C. I. (1999). Rifins: A second family of clonally variant proteins expressed on the surface of red cells infected with *Plasmodium falciparum. Proceedings of the National Academy of Sciences of the United States of America, 96*, 9333–9338.

Lavazec, C., Sanyal, S., & Templeton, T. J. (2006). Hypervariability within the Rifin, Stevor and Pfmc-2TM superfamilies in *Plasmodium falciparum. Nucleic Acids Research, 34*, 6696–6707.

Lee, G. U., Kidwell, D. A., & Colton, R. J. (1994). Sensing discrete streptavidin biotin interactions with atomic-force microscopy. *Langmuir, 10*, 354–357.

Leech, J. H., Barnwell, J. W., & Miller, L. H. (1984). Identification of a strain-specific malarial antigen exposed on the surface of *Plasmodium falciparum*-infected erythrocytes. *The Journal of Experimental Medicine, 159*, 1567.

Lowe, B. S., Mosobo, M., & Bull, P. C. (1998). All four species of human malaria parasites form rosettes. *Transactions of the Royal Society of Tropical Medicine and Hygiene, 92*, 526.

Mackinnon, M. J., Walker, P. R., & Rowe, J. A. (2002). *Plasmodium chabaudi*: Rosetting in a rodent malaria model. *Experimental Parasitology, 101*, 121–128.

McRobert, L., Preiser, P., Sharp, S., Jarra, W., Kaviratne, M., Taylor, M. C., … Sutherland, C. J. (2004). Distinct trafficking and localization of STEVOR proteins in three stages of the *Plasmodium falciparum* life cycle. *Infection and Immunity, 72*, 6597–6602.

Nash, G. B., Cooke, B. M., Carlson, J., & Wahlgren, M. (1992b). Rheological properties of rosettes formed by red blood cells parasitized by *Plasmodium falciparum. British journal of Haernatoloqy, 82*, 757–763.

Nash, G. B., Cooke, B. M., Marsh, K., Berendt, A., Newbold, C., & Stuart, J. (1992a). Rheological analysis of the adhesive interactions of red blood cells parasitized by *Plasmodium falciparum. Blood, 79*, 798–807.

Niang, M., Bei, A. K., Madnani, K. G., Pelly, S., Dankwa, S., Kanjee, U., … Preiser, P. R. (2014). STEVOR is a *Plasmodium falciparum* erythrocyte binding protein that mediates merozoite invasion and rosetting. *Cell Host & Microbe, 16*, 81–93.

Niang, M., Yam, X. Y., & Preiser, P. R. (2009). The *Plasmodium falciparum* STEVOR multigene family mediates antigenic variation of the infected erythrocyte. *PLoS Pathogens*, e1000307.

Rowe, J. A., Moulds, J. M., Newbold, C. I., & Miller, L. H. (1997). *Plasmodium falciparum* rosetting mediated by a parasite-variant erythrocyte membrane protein and complement-receptor 1. *Nature, 388*, 292–295.

Rowe, A., Obeiro, J., Newbold, C. I., & Marsh, K. (1995). *Plasmodium falciparum* rosetting is associated with malaria severity in Kenya. *Infection and Immunity Journal, 63*, 2323–2326.

Rowe, J. A., Obiero, J., Marsh, K., & Raza, A. (2002). Short report: Positive correlation between rosetting and parasitemia in *Plasmodium falciparum*

clinical isolates. *The American Journal of Tropical Medicine and Hygiene, 66*, 458–460.

Sanyal, S., Egee, S., Bouyer, G., Peerot, S., Safeukui, I., Bischoff, E., … Lavazec, C. (2012). *Plasmodium falciparum* STEVOR proteins impact erythrocyte mechanical properties. *Blood, 119*, e1–e8.

Shi, H., Zhou, L., Ang, L., Jing, Y., Alvin, G. L. C., Kevin, S. W. T., … Lim, C. T. (2013). Life cycle-dependent cytoskeletal modifications in *Plasmodium falciparum* infected erythrocytes. *PLoS One, 8*(4), e61170.

Subudhi, A. K., Boopathi, P. A., Pandey, I., Kohli, R., Karwa, R., Middha, S., … Das, A. (2015). *Plasmodium falciparum* complicated malaria: Modulation and connectivity between exportome and variant surface antigen gene families. *Molecular and Biochemical Parasitology, 201*, 31–46.

Tiburcio, M., Niang, M., Deplaine, G., Perrot, S., Bischoff, E., Ndour, P. A., … Lavazec, C. (2012). A switch in infected erythrocyte deformability at the maturation and blood circulation of *Plasmodium falciparum* transmission stages. *Blood, 119*, 172–180.

Udomsangpetch, R., Brown, A. E., Smith, C. D., & Webster, H. K. (1991). Rosette formation by *Plasmodium coatneyi*-infected red blood cells. *The American Journal of Tropical Medicine and Hygiene, 44*, 399–401.

Warimwe, G. M., Fegan, G., Musyoki, J. N., Newton, C. R., Opiyo, M., Githinji, G., … Bull, P. C. (2012). Prognostic indicators of life-threatening malaria are associated with distinct parasite variant antigen profiles. *Science Translational Medicine, 4*, 129ra45.

Wickert, H., Göttler, W., Krohne, G., & Lanzer, M. (2004). Maurer's cleft organization in the cytoplasm of *Plasmodium falciparum*-infected erythrocytes: new insights from three-dimensional reconstruction of serial ultrathin sections. *European Journal of Cell Biology, 83*, 567–582.

Wirth, D. F. (2002). The parasite genome biological revelations. *Nature, 419*, 495.

Xu, X., Efremov, A. K., Li, A., Lai, L., Dao, M., Lim, C. T., … Cao, J. (2013). Probing the cytoadherence of malaria infected red blood cells under flow. *PLoS One, 8*, e64763.

SUPPORTING INFORMATION

Additional Supporting Information may be found online in the supporting information tab for this article.